RSC Advances

ROYAL SOCIETY OF CHEMISTRY

www.rsc.org/advances

Journal Name

ARTICLE

Fabrication of Ag/γ-Fe_2O_3@TiO_2 hollow magnetic core-shell nanospheres as a highly efficient catalyst for synthesis of β-enaminones

Hongfei Huo[a], Xinzhe Li[a], Xingchun Zhou[a], Lixin Jiao[a], Shiling Zhao[a], Le Zhang[a], Wenzhu Li[a], Shuwen Li[a] and Rong Li[a]

Received 00th January 20xx,
Accepted 00th January 20xx

DOI: 10.1039/x0xx00000x

www.rsc.org/

Herein, we describe a method to prepare hollow magnetic mesoporous spheres catalyst (Ag/γ-Fe_2O_3@meso-TiO_2) . The core-shell strategy efficiently prevents the aggregation of Ag NPs in the high temperature calcination process and the leaching of Ag NPs for the catalytic reaction in a liquid phase. The catalyst is characterized by TEM, XRD, ICP-AES. Moreover, the catalyst exhibited improved activity for synthesis of β-enaminones, and it could be easily recovered by an external magnet from the reaction mixture and recycled five times without any significant loss in activity.

1. Introduction

The β-enaminones and β-enamino esters prepared by inexpensive raw materials, with very stable structural motifs are considered as valuable precursors in organic synthesis.[1] As the enaminones combine three electrophilic and two nucleophilic sites present within the enaminone functional group,[2] they were used as significant intermediates for the preparation of various heterocyclic compounds e.g. functionalized pyridin-2(1H)-ones which have been used as versatile intermediates in the synthesis of a wide range of nitrogen-containing heterocycles, such as pyridine, piperidine, quinolizidine, and indolizidine alkaloids[3] and biologically active compound[4] such as therapeutic agents[5] which were employed as synthons of different important antibacterial,[6] anti-inflammatory,[6] antitumor agent [7], dopamine auto-receptor agonists, acetylcholinestersase inhibitors, oxytocin antagonists and anticonvulsants.[8] They even served as synthons for β-aminoacids, γ-aminoalcohol which are a class of very stable compounds useful in asymmetric catalysis as a chelating agent [1]. Due to their extensive application, it is very important to search for a convenient and efficient method for the synthesis of this type of compounds. A variety of methods for the synthesis of β-enaminones and β-enamino esters were developed. Among the various methods, the condensation of 1,3-dicarbonyl compounds with amines in aromatic solvents was the most simple and straightforward route for their synthesis. However, what is tedious is that it usually required the azeotropic removal of water. A few modified procedures have been reported using various catalysts such as $Sc(OTf)_3$,[9] $CoCl_2$•$6H_2O$,[10] $ZrOCl_2$•$8H_2O$,[8] $Zn(OAc)_2$•$2H_2O$,[11] $NaAuCl_4$,[12] $SnCl_4$,[13] silica-supported antimony (III) chloride,[6] silica-supported sulfuric acid,[6] copper nanoparticles,[14] montmorillonite K10 under microwave irradiation [15] or ultrasound.[6] Although the most of reported homogenous catalysts are active for this reaction, they always have some drawbacks such as high cost, and long reaction time. Therefore, it is significant to develop an economical and easily recyclable catalyst.

It is well known that noble metal NPs (NMNPs) possess outstanding catalytic performance due to their versatile, tunable, size-, shape- and composition dependent properties [16]. However, the migration, sintering or aggregation of NMNPs constantly result in rapid decay of catalytic activity and stability. [17,18]Hence, it is crucial and challenging to develop various strategies to effectively synthetize and utilize NMNPs catalysts with desirable dimensions and improved catalytic performance. Recently, because hollow core-shell nanostructures possess desirable shell components, variable hollow space sizes, and different encapsulated species in the interior spaces, they have attracted a great deal of interest. Hollow core-shell structured materials are considered as an efficient method to inhibit undesirable sintering and aggregation of the noble metal particles.[19, 20, 21, 22, 23, 24] Because the core-shell structures have the possibilities for new physical and chemical characteristics, often different and improved from those of the constituent components, and it opens new opportunities for their successfully application in various fields like catalysis, optoelectronics, separation technology, coatings, and additives. [25]There are some reports on noble metal related core-shell materials (e.g. Pt@C, Pt@SiO_2, Pd@SiO_2) which showed superior catalytic activity in hydrogenation, oxidation, reforming and coupling reactions.[20, 22, 26, 27] If replacing the unreactive silica or carbon shells which only play a dispersion role of the active component, and the synergistic effect between the NMNPs and the shells was quite weak, with oxides, such as CeO_2 and TiO_2,[28, 29] to enhance the synergistic effect between the NMNPs and the shells may further improve the catalytic ability. TiO_2 is attractive because of its fascinating features, such as good

[a] College of Chemistry and Chemical Engineering Lanzhou University, The Key Laboratory of Catalytic engineering of Gansu Province, Lanzhou 730000, P. R. China.

† Footnotes relating to the title and/or authors should appear here.
Electronic Supplementary Information (ESI) available: [details of any supplementary information available should be included here]. See DOI: 10.1039/x0xx00000x

chemical and thermal stability, low toxicity, low cost, various. polymorphs, excellent electronic and optical properties [30]Moreover, TiO_2 possess advantageous properties and has long been recognized as an excellent support for heterogeneous catalysis. TiO_2 hollow nanostructures have many characteristics like reduced diffusion resistance, improved accessibility and high active surface area, which provide many new opportunities for the design of a highly active hollow core/TiO_2-shell materials. To our best knowledge, magnetic hollow TiO_2 shell encapsulated Ag has not been reported to date.

Herein, we report a method to stabilize Ag (0) on the surface of hollow magnetic mesoporous spheres with Ag, γ-Fe_2O_3 nanoparticles embedded in the mesoporous shell, by using Ps spheres as the templates. The fabrication procedure mainly involves six steps as shown in Fig.1. The hollow magnetic mesoporous spheres performed enhanced synergistic effect, and decreased leaching of noble metals. The catalyst was used for synthesis of β-enaminones and photoreaction.

2. Experimental section

2.1 Synthesis of the magnetite nanoparticles (Fe_3O_4 NPs)

The Fe_3O_4 NPs were prepared according to a published method with a slight modification[31]. First, 2.0 g $FeCl_2$•$4H_2O$, 4.8 g of $FeCl_3$•$6H_2O$ were added to 40 mL deionized water and stirred vigorously. Second, the above solution was purged with nitrogen gas. Then the mixture was heated to 313 K. When temperature is stable, 10 mL of ammonium hydroxide (28 wt%) was added rapidly to the solution, and it immediately turned black. The compound was kept at 363 K for 2.5 h. A black precipitate was separated by magnetic force, and washed with deionized water until the pH value of the solution was close to 7. Finally, the products were dried at 323 K overnight for further use.

2.2 Preparation of Ps

Ps latex was prepared referring to a reported method with a slight alteration.[32] It was prepared by soap-free emulsion polymerization copolymerization of styrene (20 g) and crylic acid (2.5 g) using ammonium persulfate (0.1 g) as an initiator. The reaction was carried out in nitrogen atmosphere at 343 K under magnetic stirring for 7 h. The Ps product was separated centrifugation and washed with deionized water and ethanol, respectively, then dried in vacuum at 323 K for 24 h.

2.3 Preparation of polystyrene latex with attached Fe_3O_4 NPs (Fe_3O_4/Ps)

2.5 g Ps and 1.5 g Fe_3O_4 NPs were dispersed in 60 mL and 84 mL hydrochloric acid solution (pH = 2.3), respectively. Then the former suspension was added dropwise into the latter under vigorous stirring at room temperature. After 6 h, the precipitate, i.e. Fe_3O_4 NPs attached on the surface of Ps particles, was separated from the solution with the help of an external magnet and washed several times with deionized water until the pH of the solution reached close to 7.

2.4 Loading Ag NPs onto the Fe_3O_4/Ps (Ag/Fe_3O_4/Ps)

1 g Fe_3O_4/Ps was dispersed in 80 mL distilled water and then the mixture was homogenized by ultrasonication for 30 min as part A, 0.5 g $SnCl_2$ was introduced to 100 mL 0.02 M HCl solution and then the mixture solution was homogenized by ultrasonication for 30 min as part B. Parts A and B were mixed together under ultrasonicating for 1 h. Subsequently, the particles were separated with the help of magnetic force and quickly washed three times with deionized water. Then, the particles were re-dispersed in 75 mL of fresh aqueous solution of ammoniacal silver nitrate (0.225 M) and sonicated for 1 h. At last, the precipitate was separated by magnetic force, washed three times with deionized water and then dried at 323 K for 12 h.

2.5 Production of Ag/Fe_3O_4@meso-TiO_2 NPs (Ag/γ-Fe_2O_3@meso-TiO_2)

Typically, 100 mg Ag/Fe_3O_4/Ps particles were dispersed in the mixture solution of 40 mL of ethanol and 0.25 g of cetyltrimethyl ammonium bromide (CTAB). Subsequently, the solution was homogenized by ultrasonication for 0.5 h. Then, 0.5 mL tetrabutyl titanate (TBOT) was added to the suspension under vigorous magnetic stirring. After being stirred at room temperature for 4 h, 15 mL of ethanol and 3 mL of deionized was added dropwise under vigorous stirring to the system. After that the reaction proceeded for 8 h at room temperature under stirring, the resultant particles were separated by an external magnet and washed with distilled water and ethanol, respectively. After then dried in a vacuum at room temperature overnight. After that the product was calcined at 773 K in air atmosphere for 7 h to remove Ps sphere, CTAB template and other organic species and Fe_3O_4 NPs converte into γ-Fe_2O_3 NPs. Finally, the collected sample was treated in a 20% H_2/N_2 flow (100 cm^3 min^{-1}) at 573 K (ramping rate, 5 K min^{-1}) for 3 h and passivation (0.1% O_2/N_2, 40 cm^3 min^{-1}) at ambient temperature for 3 h. The amount of Ag and Fe in the Ag/γ-Fe_2O_3@meso-TiO_2 NPs was found to be 16.0 wt% and 7.7%, based on ICP analysis.

2.6 Typical procedure for preparation of β-enaminones

For preparation of β-enaminones, 1 mmol of the amine, 2 mmol of dicarbonyl compound, 67.4 mg of the catalyst were dissolved in 5 mL of the solvent mixed in cylindrical 25 mL vessels in a reaction station equipped with magnetic stirrer bars and cooling condenser using circulation of cold water. The reaction temperature was kept in an oil bath and measured by an alcohol thermometer. After completion of the reaction, when the mixture was cooled to room temperature, the catalyst was collected by an external magnet. The solution phase was removed by syringe, and the reaction system was analyzed by GC (P.E. AutoSystem XL) or GC–MS (Agilent 6,890N/5,973N). Thereafter, the catalyst was washed with methanol and deionized water several times, respectively, after which the catalyst was dried over vacuum at 333 K to remove the remaining organics. The recovered dried solid catalyst was weighed and reused in the next run. In every run, the same ratio of the substrate-to-catalyst and solvent-to-catalyst was kept. Furthermore, Ag (15.9 wt%) content of the recycled Ag/γ-

Fe_2O_3@meso-TiO_2 catalyst remained just about the same as the fresh catalyst, indicating that Ag leaching were negligible.

2.7 Characterization of the catalyst

The synthesized catalyst was confirmed by corresponding characterization means. Powder X-ray diffraction (XRD) patterns were carried out at room temperature and performed on a Rigaku D/max-2400 diffractometer using Cu-Ka radiation as the X-ray source in the 2θ range of 10-90 °. The conversion was estimated by GC (P.E. AutoSystem XL) or GC-MS (Agilent 6,890N/5,973N). Ag content was analyzed by inductively coupled plasma (ICP) on IRIS Advantage analyzer after the sample was dissolved by HF and HNO_3. And Ti content was calculated by the removal of Ag and Fe in the sample. The morphology and microstructure of the catalyst were characterized by transmission electron microscopy (TEM). The TEM images were obtained through Tecnai G2 F30 electron microscope operating at 300 kV, and samples were obtained by placing a drop of a colloidal solution onto a copper grid and evaporating the solvent in air at room temperature. Specific surface areas were calculated by the Brunauer-Emmett-Teller (BET) method and pore sizes by the Barrett-Joyner-Halenda (BJH) methods using Brunauer-Emmett-Teller (Tristar II 3020). Inductive coupled plasma atomic emission spectrometer (ICPAES) analysis was conducted with Perkin Elmer (Optima-4300DV). Magnetic measurement of Ag/γ-Fe_2O_3/@meso-TiO_2 NPs and γ-Fe_2O_3@meso-TiO_2 NPs were investigated with a Quantum Design vibrating sample magnetometer (VSM) at room temperature in an applied magnetic field sweeping from -15 to 15 kOe.

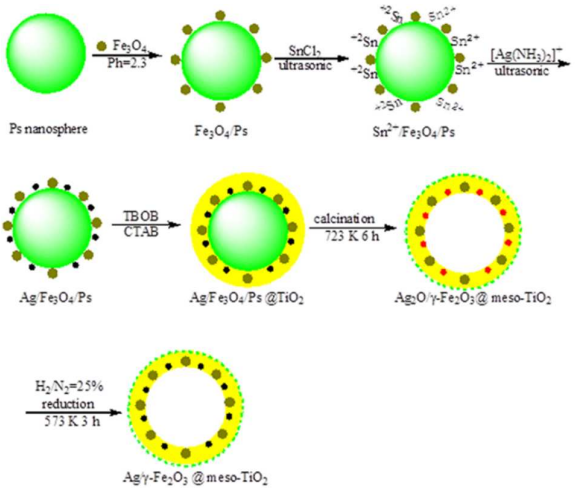

Fig.1 Scheme of the synthetic procedure for preparation of Ag/γFe_2O_3@meso-TiO_2

3. Results and discussion

3.1 Catalyst preparation and characterization

The morphologies and structures of the products at different synthetic steps were observed by TEM. Fig. 2a shows the TEM image of Ps NPs, in which well-dispersed particles with average diameter about 300 nm could be observed clearly. These Ps NPs possess functional groups (-OH, C=O) on the surface, which offer an important chemical environment for adsorbing metal ion-nanoparticles by electrostatic attraction in acidic solution. Fig. 2a is a TEM image of the Fe_3O_4/Ps composite. The Fe_3O_4 particles with an average size of about 10 to 15 nm are uniformly distributed on the surface of the Ps NPs. Fig. 2c is a TEM image of the Ag/Fe_3O_4/Ps composite. The Ag particles with an average size of about 10 to 15 nm are uniformly distributed on the surface of the Fe_3O_4/Ps NPs. Using TBOT as the TiO_2 source and CTAB as a soft template, a thin layer of mesoporous TiO_2 is coated onto the Ag/Fe_3O_4/Ps sphere. From Fig. 2d the thick of the thin layer of mesoporous TiO_2 can be seen about 30 to 40 nm. The product was collected after the calcination to remove the Ps templates and the organic groups of CTAB. Then, the Ag/γ-Fe_2O_3@meso-TiO_2 catalyst was obtained by the reduction with a hydrogen atmosphere. As shown in Fig. 2e and Fig. 2f, the TEM images show that Ag, γ-Fe_2O_3 particles were evenly coated with a layer of mesoporous shells about 30 to 40 nm thick, while the γ-Fe_2O_3 particles remained initial their cluster morphologies in the Ag/γ-Fe_2O_3@meso-TiO_2. Fig. 3e and 3f show the TEM image of the Ag/γ-Fe_2O_3@meso-TiO_2, in which well-dispersed Ag NPs with diameter about 5 to10 nm could be observed clearly. Fig. 2g is an enlarge TEM image of the Ag/Fe_3O_4/Ps composite. The Fe_3O_4 and Ag particles with an average size of about 10 to 15 nm are uniformly distributed on the surface of the Ps NPs. According to the ICP analysis, the Sn contents were below 0.2 wt%, and the Sn presence was not considered as significant in the catalytic performance of the catalyst.

The elemental composition of the Ag/γ-Fe_2O_3@meso-TiO_2 samples was determined by EDX analysis. The result shown in Fig. 3f reveals that the prepared products contain Ag, Cu, Ti, C, Sn, Fe and O. Among these elements, Cu, C and O are generally influenced by the copper network support films and their degree of oxidation, and Ti, O, Fe and Ag signals result from the Ag/γ-Fe_2O_3@meso-TiO_2. From the EDX result, the signal of Sn element was very weak, revealed that the Sn was almost completely replaced by Ag.

Fig. 3 shows the XRD patterns between 10 and 90 ° of the samples. The XRD pattern of Fe_3O_4/Ps (Fig. 3a) shows characteristic peaks of magnetite NPs, and the sharp and strong peaks confirm the products are well crystallized. In comparison with Fe_3O_4/Ps, Ag/ Fe_3O_4/Ps (Fig. 3b) exhibits four different peaks at 2θ=38.2 °, 44.3 °, 64.6 ° and 77.6 °, corresponding to the reflections of (111), (200), (220) and (311) crystal planes of silver, respectively. The XRD pattern of Ag/γ-Fe_2O_3@meso-TiO_2 (Fig. 3c) shows characteristic peaks of magnetite and TiO_2 NPs, and the sharp and strong peaks confirm Fe_3O_4 and TiO_2 in the products were transformed into γ-Fe_2O_3 and rutile, respectively. Unambiguous evidence of sliver particles in HMMS is provided via XRD. Meanwhile, the result indicating the crystalline structure of the support was well maintained in the Ag samples.

In addition, the surface area and porosity of the Ag/γ-Fe_2O_3@meso-TiO_2 hollow core-shell nanocomposites have been characterized. Fig. 5 displayed the N_2 adsorption-desorption isotherms and the corresponding pore-size

distribution curve for Ag/γ-Fe_2O_3@meso-TiO_2. The pore size was calculated by using the BJH method, as shown in the inset of Fig. 4. As a result, average pore size was about 9 nm for Ag/γ-Fe_2O_3@meso-TiO_2. The BET surface areas and the cumulative pore volumes of Ag/γ-Fe_2O_3@meso-TiO_2 were 42 m^2 g^{-1} and 0.08 cm^3 g^{-1}, respectively.

Magnetization curves revealed the superparamagnetic behavior of the magnetic NPs. The hysteresis loops of Fe_3O_4/Ps and Ag/γ-Fe_2O_3@meso-TiO_2 are shown in Fig. 5. It can be seen that the magnetic saturation values of these are 25.1 and 6.1 emu g^{-1}, respectively. The decrease of the saturation magnetization suggests the presence of the mesoporous TiO_2 shell and some silver particles inside the uniformly pore of hollow mesoporous sphere.

3.2 Catalyst testing for synthesis of β-enaminones

Acetylacetone and aniline as the representative substrate was used for the early exploration of synthesis of β-enaminones. To investigate the effect of time on product distribution, reaction times of 20, 40, 60, 80, 100, and 120 min were examined in the presence of the catalyst. The results of the influences of the reaction time on the exploration are presented in Fig. 6. With increasing the reaction time, the conversion of the reactants was increased as expected, the optimum reaction time was determined as 1 h.

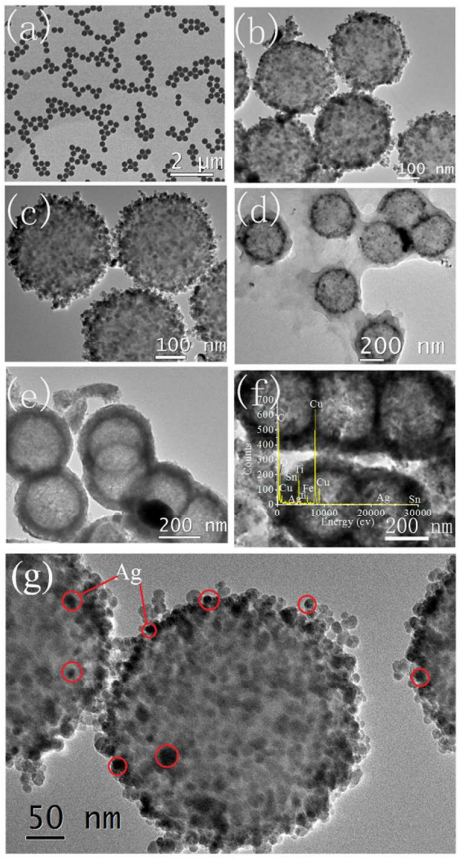

Fig. 2 TEM of PS NPs, (b) TEM of Fe_3O_4/Ps NPs, (c) TEM of Ag/Fe_3O_4/Ps, (d) TEM of Ag/Fe_3O_4/Ps@TiO_2 NPs, (e) TEM of Ag/γ-Fe_2O_3/Ps@meso-TiO_2, (f) TEM of final composite Ag/γ-Fe_2O_3@meso-TiO_2.

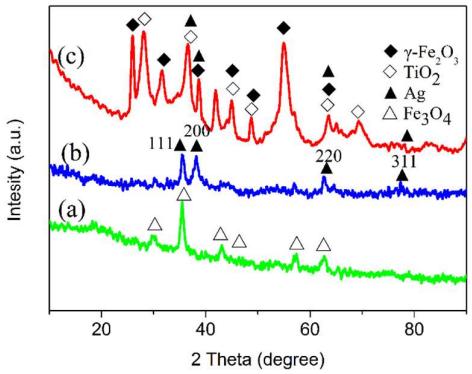

Fig. 3 XRD patterns of (a) Fe_3O_4/Ps, (b) Ag/Fe_3O_4/Ps and (c) Ag/γ-Fe_2O_3@meso-TiO_2.

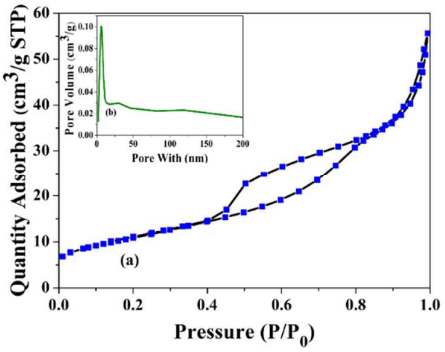

Fig. 4 N_2 adsorption/desorption isotherms and pore size distribution of Ag/γ-Fe_2O_3 @meso-TiO_2 (a) BJH adsorption dV/dlog (D) pore volume and (b) BJH desorption dV/dlog (D) pore volume

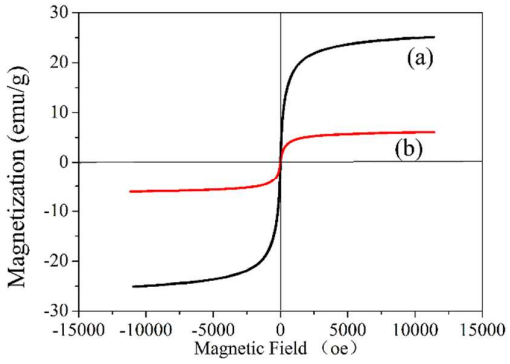

Fig. 5 Room temperature magnetization curves of (a) Fe_3O_4/Ps and (b) Ag/γ-Fe_2O_3@meso-TiO_2.

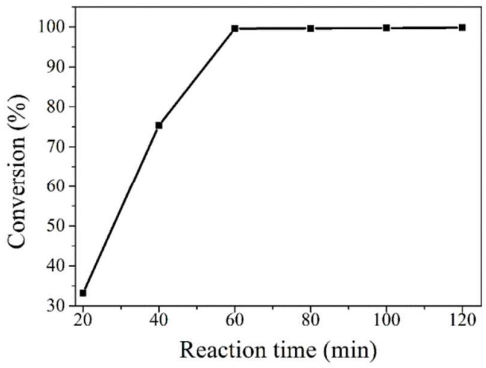

Fig. 6 Effect of reaction time on the conversion of the reaction of aniline and acetylacetone with Ag/γ-Fe_2O_3@meso-TiO_2 as catalyst. Reaction conditions: aniline 1 mmol, acetylacetone 2 mmol, the catalyst 67.4 mg, methanol 5 mL, 333 K Legend: conversion (%). Determined by GC or GC-MS.

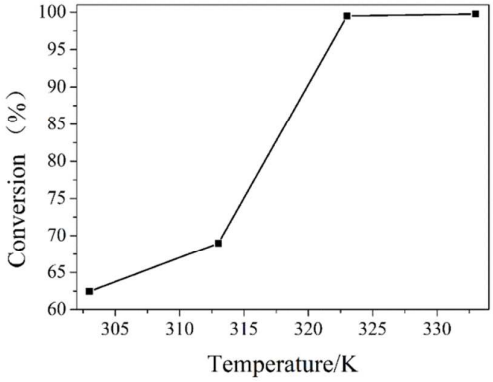

Fig. 7 Effect of temperature on the conversion of the reaction of aniline and acetylacetone with Ag/γ-Fe_2O_3@meso-TiO_2 as catalyst. Reaction conditions: aniline 1 mmol, acetylacetone 2 mmol the catalyst 67.4 mg, methanol 5 mL, 1 h. Legend: conversion (%) determined by GC or GC-MS.

The effects of the reaction temperature were shown in Fig.7. As we can see, with increasing the temperature, the conversion of aniline increased. At temperature from 303 to 323 K, the aniline conversion increased very remarkably. The optimized temperature was found at 323 K.

Table 1 presents the influence of solvent on the condensation reaction for the synthesis of β-enaminones over Ag/γ-Fe_2O_3@meso-TiO_2 at 323 K In order to promote the formation of the desired product, an excess amount of acetylacetone with respect to aniline was used (2:1). It was observed that the reaction provided a good yield with the use of methanol and DMSO as solvent, employing best results with methanol (99.5% yield) (Table 1, entries 2-8, 10, 11), which was then employed for further study. The reaction was also carried out under solvent free conditions to evolve the influence of the solvent parameter but traces of the product were detected (Table 1, entry 11). The result indicates that solvent plays a great role on the condensation

Table 1 Study of reaction parameters on reaction of aniline with acetylacetone.[a]

Entry	Solvent	Acetylaceton (mmol)	Aniline (mmol)	Yield[b] (%)
1	DMSO	2	1	94.0
2	DMSO	1	1	85.7
3	Cyclohexane	2	1	46.3
4	Ethanol	2	1	60.1
5	Acetonitrile	2	1	5.6
6	Toluene	2	1	12.0
7	THF	2	1	5.4
8	Water	2	1	42
9	Methanol	2	1	99.9>
10[c]	Methanol	1	1	99.9>
11	Solvent free	2	1	Traces

[a] Reaction conditions: solvent (5 mL), Ag/γ-Fe_2O_3@meso-TiO_2 (67.4 mg), time (1 h), reaction temperature 323 K.

[b]Yield is based on GC-MS analysis.

[c]The reaction time (2 h)

Table 2 Synthesis of various β-enaminones.[a]

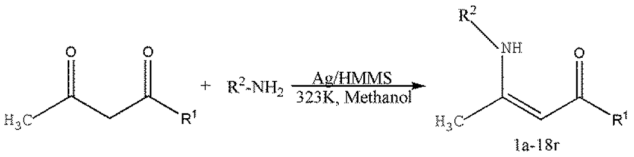

Entry	R^1	R^2	Time (h)	Product	Yield[c] (%)
1	CH_3	C_6H_5	1	1a	99.5
2	CH_3	p-$CH_3C_6H_5$	4	2b	>99.9
3	CH_3	$PhCH_2$	1	3c	>99.9 99.0[b]
4	CH_3	Cyclohexyl	1.25	4d	98.5
5	CH_3	n-C_4H_9	0.5	5e	>99.9
6	CH_3	i-C_4H_9	0.75	6f	99.7
7	OCH_3	C_6H_5	4	7g	98.2
8	OCH_3	p-$CH_3C_6H_5$	4	8h	80.6
9	OCH_3	$PhCH_2$	1	9i	>99.9
10	OCH_3	Cyclohexyl	1.25	10j	97.3
11	OCH_3	n-C_4H_9	0.5	11k	99.6
12	OCH_3	i-C_4H_9	0.75	12l	99.4
13	OC_2H_5	C_6H_5	4	13m	99.6
14	OC_2H_5	p-$CH_3C_6H_5$	4	14n	99.4
15	OC_2H_5	$PhCH_2$	1	15o	>99.9
16	OC_2H_5	Cyclohexyl	1.25	16p	99.5
17	OC_2H_5	n-C_4H_9	0.5	17q	99.7
18	OC_2H_5	i-C_4H_9	0.75	18r	96.7

[a] Reaction conditions: methanol (5 mL), dicarbonyl compound (2 mmol), amine (1 mmol), Ag/γ-Fe_2O_3@meso-TiO_2 (67.4 mg), and temperature (323 K).

[b] Yield after fifth recycle.

[c] Yield based on GC-MS analysis.

reaction and the Ag/γ-Fe_2O_3@meso-TiO_2 promote the mass diffusion and transport of reactants. Meanwhile, the molar ratio

of acetylacetone and aniline also had a significant influence on the enamination of aniline, the acetylacetone/aniline molar ratio of 1:1 gave the lower yield of desired products (Table 1, entries 2, 10).

Various amines were allowed to react with β-dicarbonyl compounds under optimized conditions in the presence of a catalytic amount of Ag/γ-Fe_2O_3@meso-TiO_2 (67.4 mg) for a certain period of time required to complete for the reactions. The results are summarized in Table 2, from which it can be observed that the reactions of amine derivatives with β-enamino ketones and esters proceeded efficiently (Table 2, entries 1-18). Acetylacetone was found to give a good yield with benzylamine, and p-toluidine (Table 2, entries 1-3). The yield of 2b was not obviously increased by the reaction time was prolonged 2 h after removed the catalyst from reaction system. The result shows that this reaction did not proceed even in the same conditions without metallic catalyst. The solution was not found the element of Fe based on ICP analysis. But the Ag content in the solution was found to be 0.4 ppm based of ICP elemental analysis, indicating that a very small amount of Ag was possibly leached. The reactions of acetylacetone with aliphatic and alicyclic amines proceeded to give excellent yields in a short period with the Ag/γ-Fe_2O_3@meso-TiO_2 as a catalyst (Table 2, entries 4-6). The reaction with aliphatic amines proceeded easily in a shorter time than aromatic amines, owning to the fact that the higher nucleophilicity of aliphatic amines as compared to aromatic amines. The addition of amines to other dicarbonyl compounds like methy acetoacetate and ethyl lacetoacetate was also studied. Methy acetoacetate and ethyl acetoacetate were found to give an excellent yield of desired products with aliphatic, aromatic and alicyclic amines under optimized reaction conditions (Table 2, entries 7-18). The catalyst can be easily recovered in a facile manner from the reaction solution by using a permanent magnet. Furthermore, the catalyst revealed a remarkable activity and was reused up to five consecutive cycles without any significant loss in catalytic activity (Table 2, entry 3).

In order to show the merit of Ag/γ-Fe_2O_3@meso-TiO_2 in comparison with other reported catalysts, we summarized some of results for preparation of entry 1 in Table 2, which shows that Ag/γ-Fe_2O_3@meso-TiO_2 is more efficient catalyst to those previously reported.

Table 3 Synthesis of 4-Phenylamino-pent-3-en-2-one (Table 2, entry 1) in the presence of different catalysts

Entry	Catalysts	The amount of Ag	Temperature (℃)	Time (h)	Yield (%)a	Ref.
1	Ag/γ-Fe_2O_3@meso-TiO_2	0.1	50	2	>99.9	
2	Ag/γ-Fe_2O_3@meso-TiO_2	0.1	60	1	>99.9	
3	Ag Np	0.1	60	8	90	1
4	$Zn(OAc)_2 \bullet 2H_2O$	0.05	60	48	86	11
5	$Zn(OAc)_2 \bullet 2H_2O$ Ag/HMMS	0.1	60	80	100	6
6		0.1	60	8	100	6

[a] Yield based on GC-MS analysis.

4. Conclusions

In conclusion, we demonstrated a successful synthesis of multicomponent Ag/γ-Fe_2O_3@meso-TiO_2 with well-defined core-shell nanostructures. According to the TEM, tiny Ag NPs were encapsulated within hollow magnetic mesoporous spheres. The Ag NPs were free of protection ligands and were well-dispersed in mesoporous spheres with a few of aggregation. Moreover, the obtained Ag/γ-Fe_2O_3@meso-TiO_2 catalyst exhibited improved catalytic activity for synthesis of β-enamino ketones or esters from β-dicarbonyl compounds, especially for synthesis of 4-Phenylamino-pent-3-en-2-one (Table 2, entry 1). Furthermore, the Ag/γ-Fe_2O_3@meso-TiO_2 catalyst had stable catalytic activity, evidenced by being extensively reused for five times without any substantial loss of activity which was mainly attributed to the small size of Ag NPs and the hollow structure of TiO_2. In addition, the structural stability of this catalyst during reaction is very well.

Acknowledgements

This work was supported by the Fundamental Research Funds for the Central Universities (lzujbky-2015-16 and lzujbky-2015-17).

References

1. K. D. Bhatte, P. J. Tambade, K. P. Dhake and B. M. Bhanage, *Catal. Commun*, 2010, **11**, 1233-1237.
2. N. D. Koduri, Z. Wang, G. Cannell, K. Cooley, T. M. Lemma, K. Miao, M. Nguyen, B. Frohock, M. Castaneda, H. Scott, D. Albinescu and S. R. and Hussaini, *J. Org. Chem.*, 2014, **79**, 7405-7414.
3. R. Zhang, D. Zhang, Y. Guo, G. Zhou, Z. Jiang and a. D. Dong, *J. Org. Chem.*, 2008, **73**, 9504–9507.
4. L. P. Fu, Q. Q. Shi, Y. Shi, B. Jiang and S. J. and Tu, *Comb. Sci.*, 2013, **15**, 135-140.
5. Y. Wang, X. B, W.-Q. Li, D. Li, Q. Zhang, Q. Liu and a. B. S. Ondon, *Org. Lett.*, 2011, **13**, 1722-1725.
6. J. Sun, Z. Dong, P. Li, F. Zhang, S. Wei, Z. Shi and R. and Li,

Mater. Chem. Phys., 2013, **140**, 1-6.
7. N. D. Eddington, D. S. Cox, M. Khurana, N. N. Salama, J. P. Stables, S. J. Harrison, A. Negussie, U. Q. T. Robert S. Taylorc, J. A. Moore, J. C. Barrow and a. K. R. Scott, *Eur. J. Med. Chem.* , 2003, **38**, 49-64.
8. Z.-H. Zhang, T.-S. Li and J.-J. Li, *Catal. Commun.*, 2007, **8**, 1615-1620.
9. J. S. Yadav, V. N. Kumar, R. S. Rao, A. D. Priyadarshini, P. P. Rao, B. V. S. Reddy and K. and Nagaiah, *J. Mol. Catal. A Chem.*, 2006, **256**, 234-237.
10. Z.-H. Zhang and J.-Y. Hu, *J. Braz. Chem. Soc.* , 2006, **17**, 1447-1451.
11. Ramandeep Kaur Vohra, J.-L. Renaud and C. Bruneau, *Collect. Czech. Chem. Commun.*, 2005, **70**, 1943-1952.
12. A. Arcadi, G. Bianchi, S. D. Giuseppe and F. Marinelli, *Green Chem.*, 2003, **5**, 64-67.
13. D. Astruc, F. Lu and J. R. Aranzaes, *Angew. Chem. Int. Ed.*, 2005, **44**, 7852-7872.
14. M. Kidwai, S. Bhardwaj, N. K. Mishra, V. Bansal, A. Kumar and S. Mozumdar, *Catal. Commun.*, 2009, **10**, 1514-1517.
15. H. T. S. Braibante, M. E. F. Braibante, G. B. Rosso and a. D. A. Oriques, *J. Braz. Chem. Soc.*, 2003, **14**, 994-997.
16. R. Güttel, M. Paul, C. Galeano and F. Schüth, *J. Catal.*, 2012, **289**, 100-104.
17. R. Narayanan and M. A. El-Sayed, *J. Am. Chem. Soc.*, 2003, **125**, 8340-8347.
18. A. Corma and H. Garcia, *Chem. Soc. Rev.*, 2008, **37**, 2096-2126.
19. Joongoo Lee, Ji Chan Park, Jung Up Bang and H. Song, *Chem. Mater.*, 2008, **20**, 5839-5844.
20. Z. Chen, Z. M. Cui, F. Niu, L. Jiang and W. G. Song, *Chem. Commun*, 2010, **46**, 6524-6526.
21. Z. Chen, Z.-M. Cui, P. Li, C.-Y. Cao, Y.-L. Hong, Z.-y. Wu and W.-G. Song, *J. Phys. Chem. C*, 2012, **116**, 14986-14991.
22. C.-H. Lin, X. Liu, S.-H. Wu, K.-H. Liu and C.-Y. Mou, *J. Phys.Chem. Lett.*, 2011, **2**, 2984-2988.
23. K. Kamata and Y. L. a. Y. Xia, *J. Am. Chem. Soc.*, 2003, **125**, 2384–2385.
24. S. Ikeda, S. Ishino, T. Harada, N. Okamoto, T. Sakata, H. Mori, S. Kuwabata, T. Torimoto and M. Matsumura, *Angew. Chem., Int. Ed.*, 2006, **45**, 7063-7066.
25. F. Caruso, *Adv. Mater.*, 2001, **13**, 11-22.
26. J. Lu, B. Fu, M. C. Kung, G. Xiao, J. W. Elam, H. H. Kung and P. C. Stair, *Science*, 2012, **335**, 1205-1208.
7. S. Liu and M. Y. Han, *Chem.–Asian J.*, 2010, **5**, 36-45.
28. F. M. S. Arrii, A. J. Renouprez and a. J. L. Rousset, *J. Am. Chem. Soc.*, 2004, **126**, 1199–1205.
29. M. Date, M. Okumura, S. Tsubota and M. and Haruta, *Angew. Chem., Int. Ed.*, 2004, **43**, 2129-2132.
30. X. Chen and a. S. S. Mao, *Chem. Rev.*, 2007, **107**, 2891-2959.
31. Y.-S. Lin and C. L. and Haynes, *Chem. Mater.*, 2009, **21**, 3979-3986.
32. P. Wang, F. Zhang, Y. Long, M. Xie, R. Li and J. and Ma, *Catal. Sci. Technol.*, 2013, **3**, 1618-1624.
33. H. Liu, S. Ji, Y. Zheng, M. Li and H. Yang, *Chin. J. Chem. Eng.*, 2013, **21**, 569-576.